Intersections of stable and unstable manifolds: the skeleton of Lagrangian chaos

F. Feudel [a], A. Witt [a], M. Gellert [a], J. Kurths [a], C. Grebogi [b], M.A.F. Sanjuán [c,*]

[a] *Institute of Physics, University of Potsdam, PF 601553, D-14469 Potsdam, Germany*
[b] *Instituto de Física, Universidade de São Paulo, Caixa Postal 66318, 05315-970 São Paulo, SP, Brasil*
[c] *Nonlinear Dynamics Group, Departamento de Matemáticas y Física Aplicadas y Ciencias de la Naturaleza, Universidad Rey Juan Carlos, Tulipán s/n, 28933 Móstoles, Madrid, Spain*

Abstract

We study Hamiltonian chaos generated by the dynamics of passive tracers moving in a two-dimensional fluid flow and describe the complex structure formed in a chaotic layer that separates a vortex region from the shear flow. The stable and unstable manifolds of unstable periodic orbits are computed. It is shown that their intersections in the Poincaré map as an invariant set of homoclinic points constitute the backbone of the chaotic layer. Special attention is paid to the finite time properties of the chaotic layer. In particular, finite time Lyapunov exponents are computed and a scaling law of the variance of their distribution is derived. Additionally, the box counting dimension as an effective dimension to characterize the fractal properties of the layer is estimated for different duration times of simulation. Its behavior in the asymptotic time limit is discussed. By computing the Lyapunov exponents and by applying methods of symbolic dynamics, the formation of the layer as a function of the external forcing strength, which in turn represents the perturbation of the originally integrable system, is characterized. In particular, it is shown that the capture of KAM tori by the layer has a remarkable influence on the averaged Lyapunov exponents.

1. Introduction

The motion of a fluid flow can be visualized by adding passive tracers into the flow and studying their dynamics. Besides important practical applications like the spread of pollutants in the atmosphere and the oceans [1], this approach provides an alternative view on pattern formation in hydrodynamic systems. This description is called Lagrangian dynamics. Unlike the Eulerian point of view it emphasizes the motion of the individual fluid particles along their pathlines. Thus, Lagrangian dynamics describes the motion of tracers injected into the fluid, that are directly visible in fluid experiments. For a steady flow, the pathlines of the individual fluid particles coincide with the streamlines of the flow. However, for a time-dependent flow they are different. Indeed it is well known that even in simple two-dimensional flows, which are periodic in time, the trajectories of the fluid particles can show very complicated, wrinkled and chaotic

---

patterns [2]. A good introduction to the topic of Lagrangian dynamics and mixing theory is given in the book by Ottino [3], while a survey of newer research developments can be found in Ref. [4]. Especially, in order to demonstrate the nice structures which are produced by the chaotic advection in experiments we refer to Refs. [5–9].

The model studied here arose in a study of passive tracers in a two-dimensional Navier–Stokes flow. A chain of driven vortices serves as the model for some fluid experiments performed by Tabeling and co-workers [10–12]. Their transitions from a laminar flow dynamics to chaos were studied on the basis of the two-dimensional Navier–Stokes equations (NSE) by Braun et al. [13]. By increasing the Reynolds number they found that the first bifurcations are in a good agreement with the experimental observations. In the following we are interested in the dynamics which appears after a Hopf bifurcation. The motion of the tracers is already chaotic even when the velocity field varies only periodically in time. To study the Lagrangian dynamics for this situation, a low-dimensional stream function model consisting of five modes was derived by Witt et al. [14]. They also studied the existence of a chaotic saddle by approximating its invariant manifolds.

In this work we start with their model but our main interest is concentrated on a better understanding of the nature and the structure of the chaotic layer and how it is modified by varying an experimentally relevant parameter, namely the amplitude of the time periodic perturbation. We study the formation process of the layer and the influence of captured KAM tori on its dynamics. It has to be noted that we look at the structure of the chaotic layer under the viewpoint that it is generated as a result of a finite time simulation. In particular, we define and determine the effective dimension, as the box counting dimension of the stable and unstable manifolds for finite duration time of the simulation. We also consider the time asymptotic limit by discussing some features of this object if the simulation time is extended asymptotically.

For this purpose the stream function model used in Ref. [14] is again reduced, keeping only the essential properties of the flow in a two-mode model. The stream function, we consider here, is then given by

$$\psi(x,y) = \psi_{(0,1)}\sin(y) + \psi_{(2,1)}\sin(2x)\sin(y), \tag{1}$$

where the indices of the stream function coefficients mark the wave number $\boldsymbol{k} = (k_x, k_y)$ of the corresponding modes. The flow consists of two components, a chain of driven vortices expressed by the second term, and a shear flow which is generated by the first term. The stream function is periodic in x with a period of π. Hence, we consider the phase space of the tracer dynamics restricted to the square, $x \in [0, \pi]$, and $y \in [0, \pi]$. In accordance with the values used in Ref. [14], and with the results of the Navier–Stokes simulations in Ref. [13], we fix the mode coefficients to $\psi_{(0,1)} = 8.35$ and $\psi_{(2,1)} = -2.55$. Moreover, in order to model the time dependence of the velocity field beyond a Hopf bifurcation, the $\psi_{(0,1)}$ coefficient is varied periodically in time as

$$\psi_{(0,1)}(t) = \psi_{(0,1)}[1 + \delta\sin(\omega t)], \tag{2}$$

where δ is a constant that measures the strength of the modulation and we set $\omega = \pi$. In accordance with the Navier–Stokes simulations the other mode coefficient $\psi_{(2,1)}$ of the driven vortices remains independent of time. For the following investigations of the Lagrangian dynamics the flow is specified by the analytic stream function model (Eq. (1)), by the special choice of the coefficients given above, and by the time variation of $\psi_{(0,1)}$ as given by Eq. (2).

The equations of motion of the passive tracer particles are given by

$$v_x = \dot{x} = \frac{\partial\psi}{\partial y}, \quad v_y = \dot{y} = -\frac{\partial\psi}{\partial x}, \tag{3}$$

which constitutes a Hamiltonian system, where $\psi(x, y, t)$ plays the role of a time-dependend Hamiltonian.

The unperturbed system of Eq. (1), i.e., when both $\delta = 0$ and $\psi_{(0,1)}$ does not depend on time, represents a stationary flow. It is integrable and resembles the phase portrait of the undamped pendulum. A homoclinic orbit encloses the vortex region and separates the vortex from the shear flow. After turning-on the periodic excitation according to Eq. (2), the fixed point is transformed into an unstable periodic trajectory which we call the primary periodic orbit. The separatrix breaks off and intersections of the stable and unstable manifolds form a complex web of chaos.

Stroboscopic maps are an appropriate technique to visualize the dynamics of periodically driven systems. In the case under consideration, Eqs. (1)–(3), it provides the visualization of the dynamics of passive tracers in physical space moving in a two-dimensional vortex flow which is varying periodically in time.

Figs. 1 and 2 show the stroboscopic map for two values of the periodic excitation, ($\delta = 0.1$ and 0.2). One clearly recognizes the different regions where the dynamics is either regular or chaotic. The motion in the vortex region is given by closed orbits which represent the dynamics on KAM tori. The regular motion of the shear flow embedding the vortex region is also reflected by smooth lines. The more interesting region addressed here is the chaotic layer which results from the break-off of the separatrix. In this layer the particles move in a non-periodic fashion.
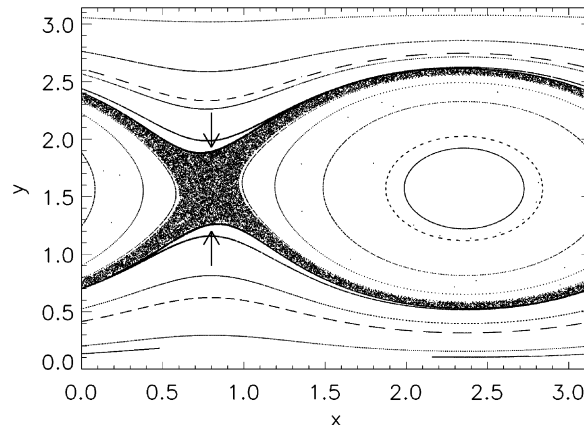
Fig. 1. Stroboscopic map of the tracer dynamics for a periodic excitation ($\delta = 0.1$), the arrays mark the two KAM tori regions which are immersed in the chaotic layer.
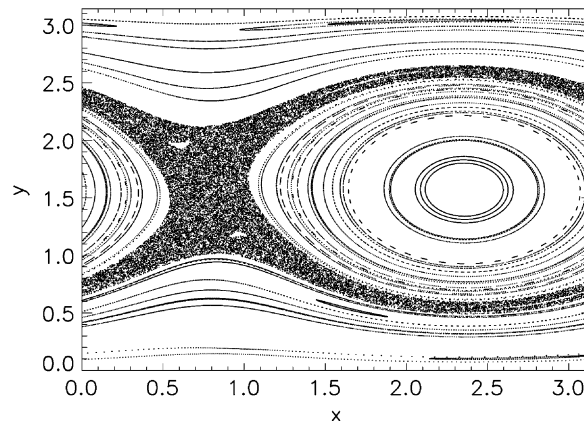

Fig. 2. Stroboscopic map of the tracer dynamics for a periodic excitation ($\delta = 0.2$).

The original homoclinic orbit breaks off for very small values of the excitation parameter δ. Due to intersections of the stable and unstable manifolds of the primary hyperbolic periodic orbit, a thin chaotic layer is formed. The layer thickness grows as δ is increased and this process is essentially ruled by the KAM theorem. In the specific situation under investigation one observes that the KAM tori which belong to the shear flow are captured by the growing layer. Fig. 1 shows an example of this process in which two surviving KAM tori regions are immersed in the chaotic layer at its upper and lower boundary. The influence of these KAM tori on the dynamics of the tracers will be discussed in Sec. 3.

By a further increase of the parameter δ, the shape of these KAM tori changes only slightly up to a value of $\delta = 0.16$. At this point a sudden drop in the size and a change in the shape of the KAM tori proceed. We do not want to give a complete explanation of this bifurcation because it happens in a very small region of the configuration space and a large zoom of the KAM tori region would be required for this purpose. In fact, as a result of a more detailed investigation, we conclude that tangencies of the stable and the unstable manifolds of a chain of periodic orbits enclosing these KAM tori regions are responsible for these changes. Due to these global bifurcations, the KAM tori shrink and get typical profiles as shown in Fig. 2.

A large zoom of the KAM tori regions shows that they are in turn surrounded by a chain of further smaller KAM tori. Repeating this procedure again and again, a self-similar structure becomes visible, which is a typical phenomenon of Hamiltonian systems. Extensive numerical investigations and a comprehensive overview on this topic, especially with regard to the KAM theory, are given in the book by Zaslavsky et al. [15].

2. Invariant sets and fractal structures

When a drop of tracers is injected in the layer, it is strongly deformed after a short time due to stretching, squeezing and folding. The generated pattern resembles that of a colored foam bath dropped into a filling bathtub that is stirred by the influent water. The drop is stretched along an unstable direction which can be identified as an approximation to the unstable manifold. In the same way, the drop is squeezed along a direction which is consistent with the stable manifold. In summary, the drop is stretched, squeezed and folded, a process involved in the dynamical creation of a fractal object. Next we discuss the nature of this mechanism.

An invariant non-attracting chaotic set, which we call a chaotic saddle, comprises the backbone of the chaotic layer. Its existence is closely related with the appearance of chaos in this region. We mentioned already about the generation of the primary periodic orbits of saddle type after the turning-on of the periodic excitation. But inside the layer there are many more periodic orbits of arbitrarily high period. All these periodic orbits possess stable and unstable manifolds. By definition, there cannot be intersections between stable manifolds and there cannot be intersections between unstable manifolds [16]. But intersection points between stable and unstable manifolds, the homoclinic and heteroclinic points, respectively, are possible. Applying the closure operation to these points gives the chaotic saddle.

Chaotic saddles for several open systems were studied in the context of scattering problems in the Refs. [17–21]. Often the sprinkling of tracer particles in the region of the chaotic saddle was applied to obtain an approximation to the unstable manifolds. Reversing the integration time for the same tracer particles, one gets the stable manifolds. As a result, the evolution of a dye of passive tracers does approximate these manifolds.

In the following we compute the manifolds of several periodic orbits of saddle type by using *DYNAMICS* [22]. Fig. 3 shows the unstable manifolds and Fig. 4 shows the stable manifolds of some of the unstable periodic orbits which we identified in the chaotic layer. We use four periodic orbits of period one, four orbits of period two, and three orbits of period three for the construction of the figures. It should be noted that the invariant sets considered here are not only one stable and one unstable manifold of one periodic trajectory but rather bundles of manifolds. In principle, in the chaotic layer exists an infinite number of periodic orbits with all periods. This number is infinite but countable. All these periodic orbits have stable and unstable manifolds and they form bundles of manifolds as suggested in Figs. 3 and 4, respectively. The intersection between stable and unstable bundles gives the chaotic saddle shown in Fig. 5. It is a fractal Cantor-like set.

However, we have to note that this structure is a result of a finite time computation. In the infinite time limit the chaos is area filling in the Hamiltonian case, and hence these stable and unstable foliations have also the full dimension of the space. However, here we are thinking of finite times, and that are the structure one gets in practice. In summary, we state that the chaotic saddle forms the backbone of the chaotic region in Hamiltonian systems, and it controls the mixing properties of the tracer dynamics in fluid experiments.
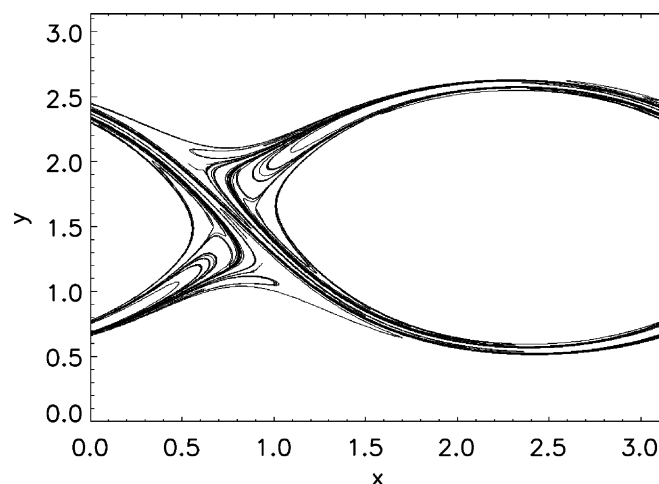

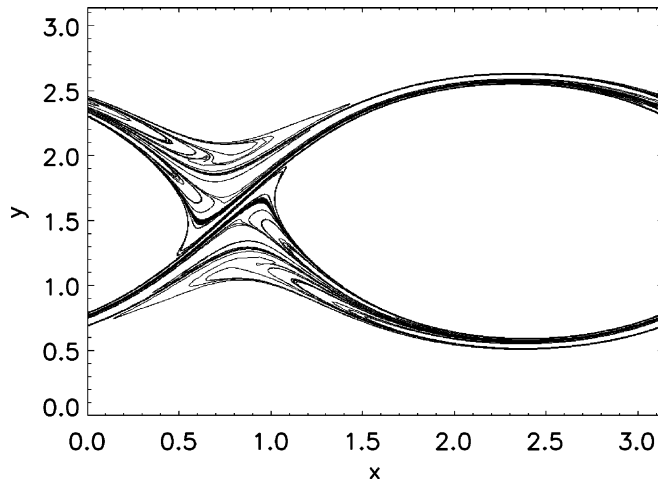Fig. 3. The unstable manifold of some of the periodic orbits ($\delta = 0.2$).

Fig. 4. The stable manifold of some of the periodic orbits ($\delta = 0.2$).
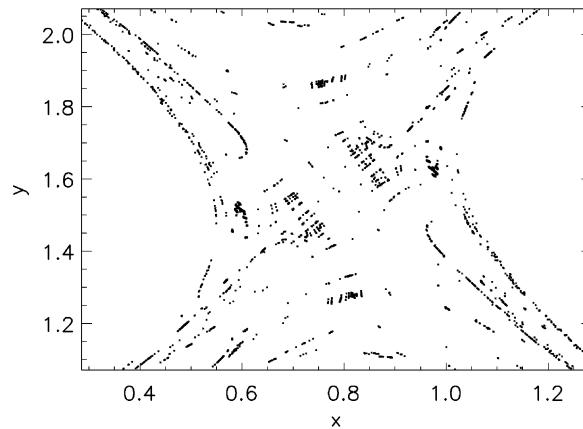

Fig. 5. Approximation of the chaotic saddle by plotting the points which have a smaller distance than a prescribed ϵ from both a stable and an unstable manifold ($\delta = 0.2$).

3. Finite time Lyapunov exponents

Lyapunov exponents are held as a standard measure to characterize the dynamics of chaotic systems. They describe the evolution of an arbitrarily chosen infinitesimal volume element v in phase space, and they measure the strength of exponential divergence or convergence in several directions. They are calculated by integrating the linearized equations

$$\dot{v} = J(t) \cdot v, \tag{4}$$

where $J(t)$ denotes the Jacobian matrix at time t. The Lyapunov exponents λ_i are the logarithms of the eigenvalues normalized by the integration time in the limit $t \to \infty$. Since the system under consideration is Hamiltonian and thus area preserving, the sum of the Lyapunov exponents is zero. We have, in our case, a periodic time-dependent stream function, which plays the role of a Hamiltonian function. The periodic forcing produces a zero exponent along the phase of the forcing direction, consequently the remaining two exponents are symmetric about zero, making the calculation of the largest exponent sufficient. In Fig. 6 this Lyapunov exponent as a function of the forcing amplitude δ is presented. In general the exponents are growing with the forcing amplitude, but around $\delta = 0.10$, there is a drop. This drop is due to the capture of two larger KAM tori regions by the expanding chaotic layer, as seen in Fig. 1. When a tracer moving chaotically in the layer approaches the KAM tori region sufficiently close, it sticks for a long time in its neighbourhood. During this time the motion looks regular and there is no exponential repulsion of neighbouring tracers [23,24]. This sticking effect is responsible for the drop of the largest Lyapunov exponent around $\delta = 0.10$.
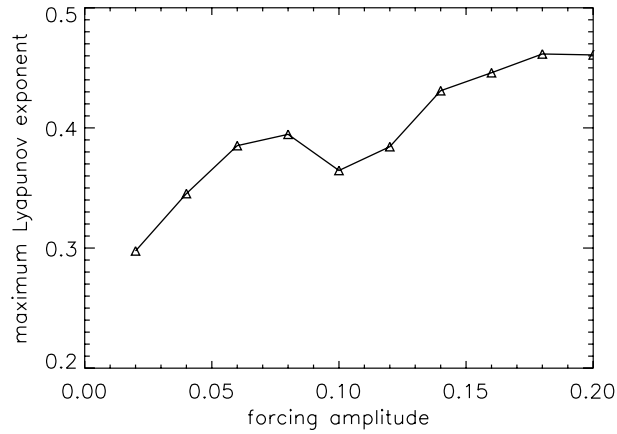
Fig. 6. Maximum Lyapunov exponent depending on the forcing amplitude δ.

The maximum Lyapunov exponent describes the average stretching rate of an infinitesimal line element in the time asymptotic limit. For finite observation times, however, the stretching rates differ from the asymptotic value. For studying the fluctuations around the mean stretching rate, distributions of finite time Lyapunov exponents are considered [25,26]. Technically, this is done by integrating Eq. (4) for a finite time t and a large set of initial conditions $v(0)$ uniformly distributed in the layer. In Fig. 7 the distribution of finite time Lyapunov exponents for different integration times t are plotted. The figure shows the longer the integration time t is, the stronger the distribution is concentrated about the (time asymptotic) Lyapunov exponent λ. Furthermore, if the finite time exponents are mapped to their initial positions one finds rather low values near the KAM-tori and rather large ones around the unstable manifold. That means that the dynamics near the KAM-tori is relatively stable, which is in good accordance with our remark made above that the dynamics may stay rather long time in the vicinity of the KAM-tori. Near the unstable manifold the dynamics is more irregular underlining the meaning of that manifold as a backbone of the dynamics.

For characterizing the convergence of the distribution of finite time exponents to the Dirac delta function, we consider the variances $\sigma^2(\lambda)$ of these distributions in terms of the simulation time t. From Fig. 8 one can infer that these variances scale as

$$\sigma^2(\lambda(t)) \sim t^{-\alpha}, \tag{5}$$

where the special value of α depends in turn on the excitation amplitude δ. We find that all values of α are greater than one, i.e., their finite time Lyapunov exponents concentrate rather fast about the asymptotic exponent λ.

A crucial point is the estimate of the dimension of the structures shown in Figs. 3–5, which are apparently fractal. However, one has to take into account that they result from finite time computations. Applying the Kaplan–Yorke
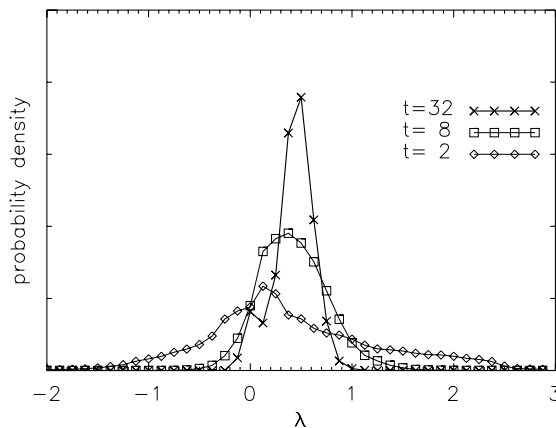

Fig. 7. Distribution of finite time Lyapunov exponents for different times t ($\delta = 0.2$).
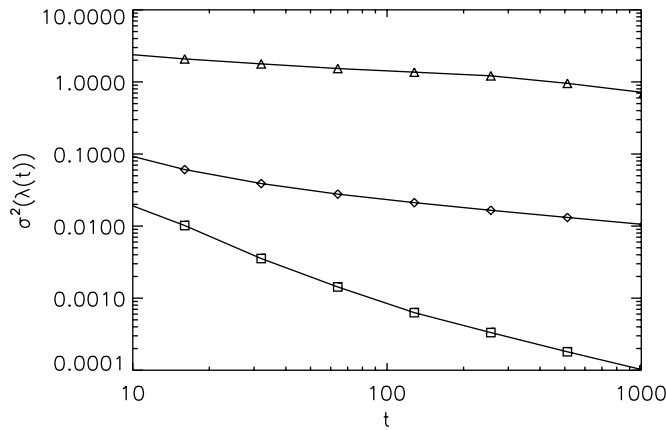
Fig. 8. Standard variances $\sigma^2(\lambda(t))$ of the Lyapunov exponents versus integration time t for $\delta = 0.1$ (triangles), $\delta = 0.15$ (squares) and $\delta = 0.2$ (diamonds) in a logarithmic plot.

fformula gives a dimension of $D_{KY} = 2$. Considering the chaotic layer in Figs. 1 and 2, it seems in fact that a typical trajectory fills out the whole layer giving this integral dimension. But both the manifolds in Figs. 3 and 4 and the chaotic saddle in Fig. 5 are not typical trajectories, because their Lebesgue measure is zero. On the other hand, they could approach arbitrary close to each point of the layer if one takes the closure. In order to demonstrate where these problems are, we estimate the box counting dimension of the unstable manifolds as a function of their computation time. Our intention is to look for any asymptotics.

For this purpose, we tracked the evolution of a line element of length 0.0002 which was placed initially on the center of the chaotic saddle, i.e., in the neighbourhood of the primary periodic orbit. It is stretched and elongated along the unstable directions, rapidly converging to the unstable manifolds. The length of the line grows exponentially. In order to retain the discrete representation of this line element, new points are added if the distance between neighbouring points exceeds a certain limit. In each time step the positions of neighbouring points are determined, and, if larger than the critical distance 0.001, new points filling this gap are added. For finite time simulation this object looks fractal like the plot of the unstable manifold in Fig. 3. In contrast to Fig. 3, this approximation to the unstable foliation contains much more points and thus allowing for a more reliable computation of its box counting dimension. In order to reduce the problem we consider the intersection with the horizontal line $y = \pi/2$ and determine the box counting dimension of this intersecting set.

Fig. 9 shows the box counting dimension versus the logarithm of the box radius ϵ for three duration times of the simulation, $t = 5T$, $6T$ and $7T$, where $T = 2\pi/\omega$ is the period of the periodic excitation according to Eq. (2). For
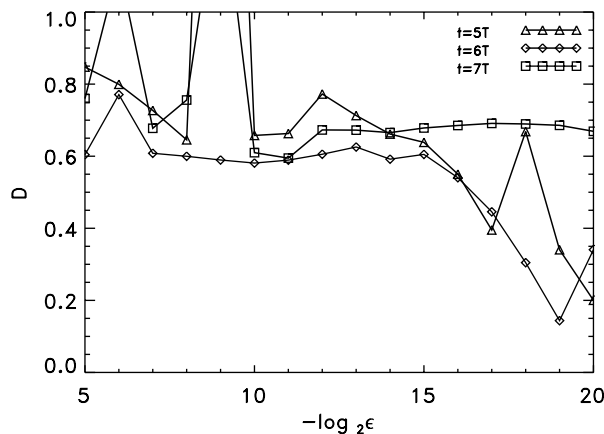

Fig. 9. The box counting dimension of the line element versus the logarithm of the box radius computed after the integration of 5, 6 and 7 time periods $T = 2\pi/\omega$.

$t = 5T$ the integration time is too short and no plateau in the corresponding curve can be identified. However, for $t = 6T$ and $t = 7T$, in both curves a plateau is clearly discernible indicating the existence of a scaling behavior over several length scales. For fractal sets the height of the plateau determines the box counting dimension. For both cases one gets a dimension of $D_0 \approx 0.6$, or equivalently, $1 + D_0 \approx 1.6$ for the dimension of the unstable manifolds. One recognizes that the scaling region is broadened with growing integration time. Additionally, it seems that it is shifted rightwards by increasing the integration time. The latter effect can be due to the fact that the system studied here is a closed system. In contrast to scattering problems where the tracers escape from the region of the chaotic saddle, here the tracers are fed back into this region. This re-entrance property inhibits a perfect scaling at the larger scales. In summary we conclude that after the finite time evolution of the line element it becomes a fractal set with a constant box counting dimension over a wider range of spatial scales.

4. A coarse-grained description of the dynamics

In the previous sections geometric properties on small scales for finite times are characterized. Now we study coarse-grained dynamic structures. The main idea of coarse-graining the dynamics is to map each trajectory into a symbol sequence. If the transformation into symbols is skillfully chosen, the properties of such symbol sequences are related to those of the underlying dynamics. Maximal equivalence between symbolic and original dynamics is reached for symbol transformations based on generating partitions. In this case the Shannon entropy of the symbol sequence coincides with the maximum Lyapunov exponent of the full dynamics [27,28].

In case of periodically forced Hamiltonian systems there are some standard approaches for defining the transformation from phase space trajectories into symbol sequences on the basis of a complicated partitioning of the stroboscopic plane [29,30]. Thus, each point of the stroboscopic plane $T = 2k\pi$, k integer, is mapped onto a symbol depending on its spatial position. In this analysis, however, a different approach is suggested. It is based on the understanding of the dynamics as an irregular switching between the motion in the shear flow and around the vortices. A symbol is produced when the passive tracer has gone through the former separatix in the x or y direction, i.e., if the line $x = \pi/4$ is encountered, the symbol "1" appears and the symbol "0" is added by reaching $y = \pi/2$. Thus the symbol "1" marks motion in the shear flow whereas a "0" symbolizes motion around the vortex. Consequently, for the motion outside the layer, one gets sequences which are constantly zero in the vortex region and constantly one in the shear flow, respectively. However, for the motion in the layer, the symbols appear rather randomly reflecting its chaoticity. We use then complexity measures as an appropriate tool to describe the structure of these symbol sequences in order to characterize the tracer dynamics in the layer.

The next step is to characterize the structure of the symbol sequences. The traditional quantity for characterizing a symbol sequence is the Shannon entropy [31]. The Shannon entropy of nth order H_n is based on the probability distribution of length-n substrings s^n (words of length n) of the symbol sequence:

$$H_n = - \sum_{s^n \in A^n, p(s^n)>0} p(s^n)\log_2 p(s^n),$$ (6)

where A^n denotes the set of all length-n words. H_n measures the average number of bits needed to specify an arbitrary word of length n in a sequence S. Their differences $h_n = H_{n+1} - H_n$, $h_0 = H_1$ quantify the mean information needed to determine the $(n + 1)$st symbol of an arbitrary word of a given sequence if the first n symbols are known. The Shannon entropy h of the system is then defined as the limit of the h_n

$$h = \lim_{n \to \infty} h_n.$$ (7)

It describes the mean information contents per symbol. In case of constant or periodic symbol sequences, h vanishes, whereas its maximum value of one is reached in the case of uncorrelated random sequences.

We have produced for the system under consideration symbol sequences of 200 000 elements with respect to different forcing amplitudes δ. For practical reasons the Shannon entropy is approximated by h_{10} here, which serves as an upper bound for h. The Shannon entropy is a measure for the averaged information per symbol. However, we need measures which are related to a time unit in order to compare them with the Lyapunov exponents. For this reason we use the normalized measures by dividing them by the time T_s, the averaged time in which a new symbol is generated during the simulation process. This time T_s is a function of the forcing amplitude δ. Additionally, the algorithmic complexity is calculated as an alternative estimator of the Shannon entropy [32]. The results are presented in Fig. 10. The figure gives a comparison of the largest Lyapunov exponent, computed in the previous Section, with the normalized Shannon entropy and the normalized algorithmic complexity resulting from the symbolic description of the dynamics. There is a qualitatively good agreement of the measures derived from the symbolic dynamics with the curve of the Lyapunov
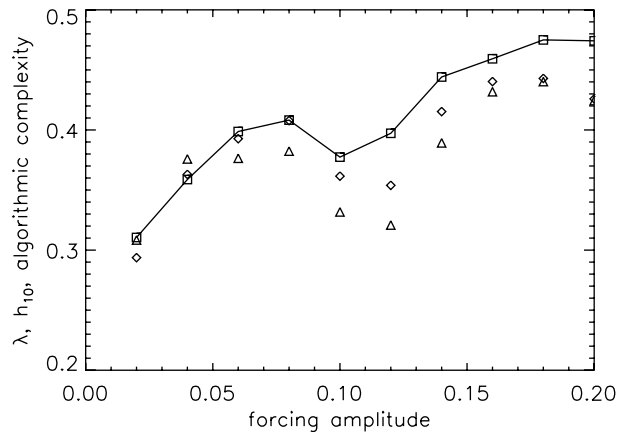
Fig. 10. Comparison of the largest Lyapunov exponent (squares) with the normalized Shannon entropy h_{10}/T_s (triangles) and with the normalized algorithmic complexity (diamonds) depending on the forcing amplitude δ.

exponents. In particular, the drop due to the KAM tori effect is also reflected by these measures. This confirms the appropriateness of our choice of the transformation into symbols from the viewpoint of characterizing the nonlinear dynamics. Although we are not able to prove that the chosen transformation into symbols is based on a generating partition, these results show that this transformation might be considered as to be appropriate. Furthermore, we like to mention that this symbolic transformation is rather robust and easily applicable to experimental data.

5. Conclusions

We have studied a two-mode time-dependent stream function derived from a two-dimensional Navier–Stokes flow. In particular, a thin chaotic layer is formed due to the intersections of the invariant manifolds. Moreover it is worth to emphasize once again that in time-dependent Hamiltonian systems the hyperbolic periodic orbits play an essential role in the generation of chaos. In fluid dynamics this mechanism controls the mixing process [33]. Firstly, the fluid is compressed and stretched along the eigendirections of the hyperbolic periodic orbits. Secondly, they are the source of stable and unstable manifolds which in turn are the germs of the chaotic region. The hyperbolic orbits in relation with their invariant manifolds and in an interplay with the KAM tori region establish a complex dynamics for the passive tracers. Especially in finite times, pretty structures of fractal nature appear as image of these invariant objects.

We have also carried out quantitative measures of the chaoticity of the fluid flow with the help of the computation of the finite-time Lyapunov exponents and the box counting dimensions of the invariant manifolds. Finally, a symbolic dynamics description is found to be an appropriate transformation from trajectories into symbol sequences, showing an excellent agreement between their finite time Lyapunov exponents and the normalized Shannnon entropies.

In summary, by using different techniques from nonlinear dynamics, we have characterized the Lagrangian chaos present in the fluid flow that is generated by the chaotic saddle formed by the intersections of the invariant manifolds associated to unstable periodic orbits inside the chaotic layer.

References

[1] Holton J, Haynes PH, McIntyre ME, Douglas AR, Rood RB, Pfister L. Stratosphere–troposphere exchange. Rev Geophys 1995;33:403–39.

[2] Aref H. Stirring by chaotic advection. J Fluid Mech 1984;143:1–21.
[3] Ottino JM. The theory of mixing: stretching, chaos and transport. Cambridge: Cambridge University Press; 1989.
[4] Aref H, editor. Chaos applied to fluid mixing. Chaos, Solitons & Fractals, vol. 4. Oxford: Pergamon Press; 1994. p. 745–1116.
[5] Sommerer JC, Ku H-C, Gilreath HE. Experimental evidence for chaotic scattering in a fluid wake. Phys Rev Lett 1996;77:5055–8.
[6] Fountain G, Khakhar D, Ottino J. Visualization of three-dimensional chaos. Science 1999;281:683–6.
[7] Aref H. Order in chaos. Nature 1999;401:756–8.
[8] Rothstein D, Henry E, Gollub J. Persistent patterns in transient chaotic fluid mixing. Nature 1999;401:770–2.
[9] Fountain G, Khakhar D, Mezić I, Ottino J. Chaotic mixing in a bounded three-dimensional flow. J Fluid Mech 2000;417:265–301.
[10] Tabeling P, Perrin B, Fauve S. Instability of a linear array of forced vortices. Europhys Lett 1987;3:459–65.
[11] Tabeling P, Cardoso O, Perrin B. Chaos in a linear array of vortices. J Fluid Mech 1990;213:511–30.
[12] Willaime H, Cardoso O, Tabeling P. Spatiotemporal intermittency in lines of vortices. Phys Rev E 1993;48:288–95.
[13] Braun R, Feudel F, Guzdar P. The route to chaos for a two-dimensional externally driven flow. Phys Rev E 1998;58:1927–32.
[14] Witt A, Braun R, Feudel F, Grebogi C, Kurths J. Tracer dynamics in a flow of driven vortices. Phys Rev E 1999;59:1605–14.
[15] Zaslavsky GM, Sagdeev RZ, Usikov DA, Chernikov AA. Weak chaos and quasi-regular patterns. Cambridge: Cambridge University Press; 1991.
[16] Lichtenberg AJ, Lieberman MA. Regular and chaotic dynamics. New-York: Springer-Verlag; 1992.
[17] Hsu GH, Ott E, Grebogi C. Strange saddles and the dimension of their invariant manifolds. Phys Lett A 1988;127:199–204.
[18] Péntek A, Toroczkai Z, Tél T, Grebogi C, Yorke JA. Fractal boundaries in open hydrodynamical flows: signatures of chaotic saddles. Phys Rev E 1995;51:4076–88.
[19] Toroczkai Z, Károlyi G, Péntek A, Tél T, Grebogi C, Yorke JA. Wada dye boundaries in open hydrodynamical flows. Phys A 1997;239:235–43.
[20] Sanjuan MAF, Kennedy J, Ott E, Yorke JA. Indecomposable continua and the characterization of strange sets in nonlinear dynamics. Phys Rev Lett 1997;78:1892–5.
[21] Sanjuan MAF, Kennedy J, Grebogi C, Yorke JA. Indecomposable continua in dynamical systems with noise: fluid flow past an array of cylinders. Chaos, Solitons & Fractals 1997;7:125–38.
[22] Nusse H, Yorke JA. Dynamics: numerical exploration. Berlin: Springer Verlag; 1994.
[23] Chirikov B. A universal instability of many-dimensional oscillator systems. Phys Rep 1979;52:263–379.
[24] Abdullaev S. Structure of motion near saddle points and chaotic transport in Hamiltonian systems. Phys Rev E 2000;62:3508–28.
[25] Eckmann J-P, Procaccia I. Fluctuations of dynamical scaling indices in nonlinear systems. Phys Rev A 1986;34:659–61.
[26] Brandenburg A, Klapper I, Kurths J. Generalized entropies in a turbulent dynamo. Phys Rev E 1995;52:4602–5.
[27] Grassberger P, Kantz PH. Generating partitions for the dissipative Hénon map. Phys Lett A 1985;113:235–8.
[28] Kurths J, Voss A, Saparin P, Witt A, Kleiner H, Wessel N. Quantitative analysis of heart rate variability. Chaos, Solitons & Fractals 1995;5:88–94.
[29] Christiansen F, Politi A. Generating partition for the standard map. Phys Rev E 1995;51:R3811–4.
[30] Christiansen F, Politi A. Symbolic encoding in symplectic maps. Nonlinearity 1996;9:1623–40.
[31] Shannon CE, Weaver W. The mathematical theory of communication. Urbana: Univ. of Illinois Press; 1949.
[32] Lempel A, Ziv J. Complexity of finite sequences. IEEE Trans Inf Theory 1976;22:75–81.
[33] Anderson P, Galaktionov O, Peters G, van de Vosse F, Meijer H. Analysis of mixing in three-dimensional time-periodic cavity flows. Science 1999;386:149–66.